EUROPEAN JOURNAL OF COMPUTATIONAL MECHANICS
2018, VOL. 27, NO. 2, 163–185
https://doi.org/10.1080/17797179.2018.1484208

Taylor & Francis
Taylor & Francis Group

On the shell thickness-stretching effects using seven-parameter triangular element

M. Rezaiee-Pajand, Amir R. Masoodi and E. Arabi

Department of Civil Engineering, Ferdowsi University of Mashhad, Mashhad, Iran

ABSTRACT

In this study, two triangular shell element having three and six nodes are presented for geometrically nonlinear analysis of thin and thick shell structures. The main contribution of this research is to achieve efficient seven-parameter shell elements, which can be employed in the geometrically nonlinear analysis of thin, moderately thick and thick shell structures. The present formulation employs seven degrees of freedom at each node of elements. Owing to this fact, thickness variation is considered as degree of freedom. This formulation makes it possible to investigate the effect of thickness-stretching and calculate its value for all types of shells, especially thick ones. To avoid shear and membrane locking, the Mixed Interpolation of Tensorial Components (MITC) is adopted in formulation. In addition, the fully 3D constitutive relation is used due to consideration of the thickness variation. Furthermore, several nonlinear benchmark problems are studied to illustrate the accuracy and ability of authors' scheme in comparison with that of other references. Consequently, the effects of thickness extension on the results will be investigated in most of them by presenting the related equilibrium paths of shells with different values of thickness.

ARTICLE HISTORY
Received 9 August 2017
Accepted 31 May 2018

KEYWORDS
Triangular shell element; seven-parameter formulation; thickness variation; MITC method; thick shell; geometrically nonlinear analysis

1. Introduction

In the past decades, finite-element method has been widely developed to analyse the arbitrary thin and thick shell structures. In order to achieve a more realistic behaviour of such structures, especially in the nonlinear analysis, it is essential to utilise a proper mathematical model, including 3D effects. Triangular shell element is still an interesting subject to develop, because such element has powerful ability to analyse the structures with general geometrical shape, especially curved bodies. Furthermore, considering new effects, such as, complexity of the thickness-stretching is interesting. Up to this date, the most important developments of shell structure analyses are based on the finite-element method. Hence, developing a reliable and efficient new element is the main aim of this study.

CONTACT M. Rezaiee-Pajand rezaiee@um.ac.ir

So far, many curved quadrilateral and triangular degenerated shell elements have been proposed. In addition, various formulations have been developed in conjunction with them for the geometrically nonlinear structural analysis. For the first time, the degenerated shell element theory was obtained by Ahmad, Irons, and Zienkiewicz (1970)for analysing the curved shell elements. Moreover, the research of Liu, Law, Lam, and Belytschko (1986)among the many other studies expressed the same procedure for the shell analysis. Furthermore, the books of Bathe (1982; Chapelle & Bathe, 2011) and Crisfield (1986) have explained the general developments of the degenerated shell element procedure.

In 2007, a research was performed about employing an efficient co-rotational formulation to develop a curved six-node triangular shell element by Li and Vu-Quoc (2007). The rigid-body translations and rotations were obtained in the global coordinate system to calculate the strain energy. They also employed the interpolation of strain to alleviate the shear and membrane locking. In another research, a particular linearisation method was proposed to develop the updated Lagrangian formulation for the geometrically nonlinear analysis of shell structures by Kordkheili, Naghdabadi, and Jabbarzadeh (2008). They utilised Green-Lagrange strain and the second Piola–Kirchhoff stress at two second-order functions in terms of a through-the-thickness parameter. Furthermore, Dung and Wells (2008)proposed a finite-element formulation for the geometrically nonlinear analysis of thin shells. The rotation degrees of freedom were not defined in their formulation. Development of a four-node flat quadrilateral shell element for geometrically nonlinear analysis was performed by Boutagouga, Gouasmia, and Djeghaba (2010). They used in-plane rotational degree of freedom to improve the in-plane behaviour of the element. In their formulation, six degrees of freedom were employed in each node of the element. Nguyen-Van, Nguyen-Hoai, Chau-Dinh, and Tran-Cong (2015)studied the nonlinear behaviours of plates and shells using an efficient four-node flat element. The von Kármán large deflection theory and the Total Lagrangian formulation were employed in their research. Jung and Han (2015) proposed another scheme for a nine-node shell element for geometrically nonlinear analysis. Their solution was based on the Total Lagrangian formulation. In addition, a refined first-order shear deformation theory, for the thin and thick shells, was developed in their studies.

One of the powerful procedures in deriving the free-locking elements is the Mixed Interpolation of Tensorial Components (MITC) method. This scheme found its roots in the research of Dvorkin and Bathe (1984), where a four-node general shell element, called MITC4, was proposed. In another research, 9-node and 16-node general shell elements were studied by Bucalem and Bathe (1993). They used MITC formulation to develop their shell elements. A review of using MITC method to investigate three general shell elements, including MITC4, MITC8 and MITC4-TLH, was performed by Dvorkin

(1995). Based on this technique, a simple procedure was employed by Lee and Bathe. They presented an isotropic triangular shell element by using the MITC approach. The element was a six-node element with five degrees of freedom per node (Lee & Bathe, 2004). Recently, a new triangular shell element enriched by the bubble functions, which was formerly presented in Lee, Lee, and Bathe (2014), was employed by Jeon, Lee, Lee, and Bathe (2015) to perform geometrically nonlinear analysis. They did not incorporate the effect of thickness variation in their formulation. One of the newest researches about MITC shell element was performed by Rezaiee-Pajand, Arabi, and Masoodi (2018). They formulated an efficient locking-free triangular shell element to employ in the nonlinear analysis. It should be mentioned that thickness-stretching effects were not included in their study. Thermo-mechanical analysis of shell structures was implemented by Masoodi and Arabi (2018). They used a six-node triangular shell element which was formulated based on the MITC method for the geometrically nonlinear analysis of thin and moderately thick shell structures. They also did not consider thickness variation in their research.

In many researches, the effects of normal strain along the thickness of shell elements are ignored. When the thick shell structures are analysed, it is required to take the effects of thickness variations into account. One of the methods to consider the variation of thickness is utilising solid elements. Experiences have demonstrated that using general shell elements, based on the degenerated shell theory, are more applicable and suitable and needs less computational efforts. A geometrically nonlinear formulation was proposed for the 3D solid-shell by Surana (1982). The proposed element was an essential work connecting between the solid and shell elements. In another research, a complete 3D constitutive law without modification was directly proposed by Buchter, Ramm, and Roehl (1994), including a linear varying shell thickness. They utilised a seven-parameter theory. Moreover, El-Abbasi and Meguid (2000) developed a new seven-parameter shell element for analysis of shell structures accounting for through-thickness deformation. In addition, a fully nonlinear analysis of shell structures using multi-parameter shell element was performed by Pimenta, Campello, and Wriggers (2004). They proposed a triangular shell element with thickness variation as a nodal degree of freedom. Coda and Paccola (2007)employed a new finite-element shell formulation based on the non-conventional nodal parameters. These investigators considered nodal parameters as nodal positions and generalised vector components comprising through-thickness changes and director cosines. To perform the geometrically nonlinear analysis, Arciniega and Reddy (2007) developed a tensor-based finite-element formulation of seven-parameter higher-order quadrilateral shell element. Kim and Bathe (2008) proposed a popular shell element MITC4 for incompressible analyses. The

element was enriched by a fully 3D stress–strain description, appropriate for through-thickness displacements and pressure degrees of freedom.

Based on the stated literature review, some researches were implemented about the formulation of seven-parameter shell element. However, developing an efficient triangular shell element which can analyse thin to thick shell structures, using fewer numbers of element and without locking phenomena, has not been suggested yet. Thus, studying the geometrically nonlinear analysis of thin and thick shells is the main objective this research. In addition, the authors propose two efficient, free-locking and seven-parameter triangular shell elements having three and six nodes to be able to analyse complicated shell structures. It is worth mentioning that seven degrees of freedom, including transitional, rotational and thickness variation are assigned to each node of elements. Accordingly, the thickness variation is considered as the nodal degrees of freedom. To obtain the stiffness matrix, it is necessary to use fully 3D stress–strain constitutive matrix in formulation. One of the important contributions of this study is using the MITC approach which makes it possible that the proposed elements behave without shear, membrane and thickness locking. The authors only compared their proposed elements in regard to displacement results. In order to show the ability of proposed formulation for analysing large displacement and rotation problems, some popular nonlinear benchmarks are studied as well. Consequently, the obtained responses are reported for two cases. Firstly, nonlinear analysis of thin shell structures is carried out to demonstrate that the elements are locking-free. Afterwards, the responses are provided for thick shells to indicate the role of thickness-stretching on the equilibrium paths.

2. Geometric and kinematic description

In this section, the geometric and kinematic relations of thick shells are presented. The elements used in this study are three- and six-node triangular shell elements as depicted in Figure 1(a,b), respectively.

Each element is considered to have 7 degrees of freedom per shell node: Three translations, two rotations and two degrees of freedom for thickness change. The shell geometry at time 0 is interpolated as follows:

$$ {}^{0}\vec{x}(r,s,t) = \sum_{i=1}^{m} h_i(r,s)\,{}^{0}\vec{x}_i + \frac{t}{2}\sum_{i=1}^{m} {}^{0}a_i h_i(r,s)\,{}^{0}\vec{V}_n^i \tag{1} $$

where $h_i(r,s)$is the shape function. Moreover, a_i and $\vec{V}_n^i$ are the thickness and the director vector at node i, respectively. The natural coordinates are depicted by r, s and t. Moreover, m defines the number of element nodes. After deformation, the shell geometry expresses in the following form:

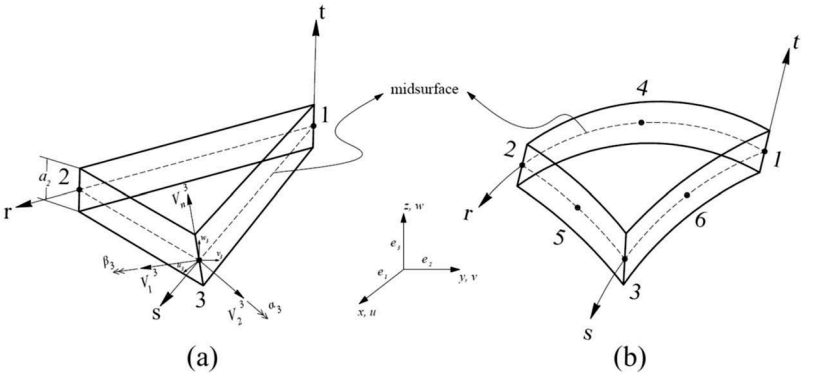

Figure 1. Geometry of triangular shell element: (a) three-node element and (b) six-node element.

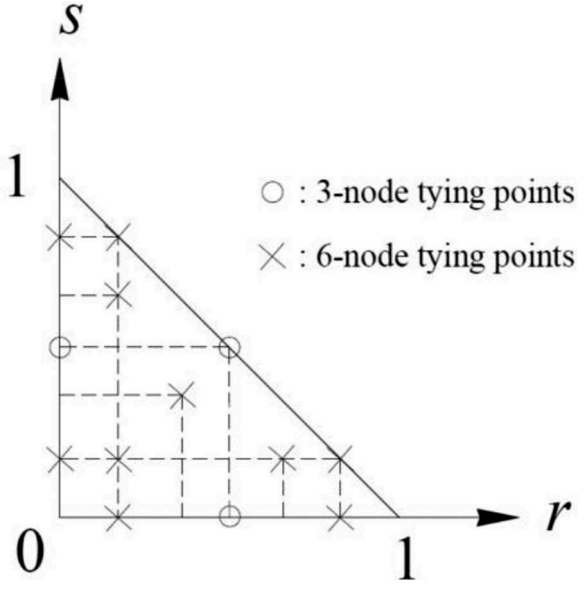

Figure 2. The position of tying points for three- and six-node elements.

$$ {}^{t}\vec{x}(r,s,t) = \sum_{i=1}^{m} h_i(r,s)\,{}^{t}\vec{x}_i \;+\; \frac{t}{2}\sum_{i=1}^{m} {}^{t}a_i h_i(r,s)\,{}^{t}\vec{V}_n^{\,i} \;+\; t^2 \sum_{i=1}^{m} {}^{0}a_i h_i(r,s)\,{}^{t}Q_n^{i}\,\overset{t\to i}{V}_n \tag{2} $$

where $\overset{t\to i}{V}_n$ and ${}^{t}a_i$ are the director vector, and thickness of node i corresponding to the configuration at time t, respectively. Additional degree of freedom corresponding to quadratic displacement functions is presented by ${}^{t}Q_n^{i}$. Based on Equation (2), the following incremental displacement vector is obtained:

$$\begin{aligned}
&\vec{u}(r,s,t) = {}^{t+\Delta t}\vec{x}(r,s,t) - {}^{t}\vec{x}(r,s,t)\\
&\vec{u}(r,s,t) = \sum_{i=1}^{m} h_i(r,s)\overrightarrow{u_i} + \frac{t}{2}\sum_{i=1}^{m} h_i\left({}^{t+\Delta t}a_i \overset{t+\Delta t\rightarrow i}{V_n} - {}^{t}a_i \overset{t\rightarrow i}{V_n}\right)\\
&\quad + t^2\sum_{i=1}^{m} h_i(r,s)^0 a_i\left({}^{t+\Delta t}Q_n^i \overset{t+\Delta t\rightarrow i}{V_n} - {}^{t}Q_n^i \overset{t\rightarrow i}{V_n}\right)
\end{aligned} \tag{3}$$

By using the next expressions, Equation (3) can be extended in terms of the degrees of freedom:

$$\begin{aligned}
\overrightarrow{u_i} &= u_i\overrightarrow{e_1} + v_i\overrightarrow{e_2} + w_i\overrightarrow{e_3}\\
{}^{t+\Delta t}a_i - {}^{t}a_i &= {}^{0}a.\Delta_a^i \qquad {}^{t+\Delta t}Q_n^i - {}^{t}Q_n^i = q_n^i
\end{aligned} \tag{4}$$

where incremental translations are given in global coordinate. It should be noted that the incremental thickness change, which is normalised with respect to the initial thickness, is defined by Δ_a^i. To obtain the director vector at time $t + \Delta t$, from that at the configuration at time t, the rotation matrix ${}_t^{t+\Delta t}\Phi^{\mathrm{i}}$ should be utilised:

$$\overset{t+\Delta t\rightarrow}{V_j^i} = t + \Delta t\,{}_t\Phi^{\mathrm{i}}\overset{t\rightarrow}{V_j^i} \qquad (j = 1,2,n) \tag{5}$$

The series expansion of the finite rotation tensor is as follows:

$${}_t^{t+\Delta t}\Phi^{\mathrm{i}} = \mathrm{I}_3 + {}_t^{t+\Delta t}\Theta^{\mathrm{i}} + \frac{1}{2!}\left({}_t^{t+\Delta t}\Theta^{\mathrm{i}}\right)^2 + \frac{1}{3!}\left({}_t^{t+\Delta t}\Theta^{\mathrm{i}}\right)^3 + \ldots\ldots\ldots \tag{6}$$

where I_3 is the 3×3 identity matrix, and ${}_t^{t+\Delta t}\Theta^i$ is the skew-symmetric matrix, including the rotational degrees of freedom. After some simplification, the following relation is in hand:

$${}^{t+\Delta t}\overrightarrow{V}_n^i - \overset{t\rightarrow}{V_n^i} \cong \beta_i \overset{t\rightarrow}{V_1^i} - \alpha_i \overset{t\rightarrow}{V_2^i} - \frac{1}{2}\left({\alpha_i}^2 + {\beta_i}^2\right)\overset{t\rightarrow}{V_n^i} \tag{7}$$

where α_i and β_i are the incremental rotational degrees of freedom about $\overset{t\rightarrow i}{V_1}$ and $\overset{t\rightarrow i}{V_2}$, respectively. In addition, $\overset{t\rightarrow i}{V_1}$ and $\overset{t\rightarrow i}{V_2}$ are unit vectors orthogonal to $\overset{t\rightarrow i}{V_n}$ and have the next relations:

$$\begin{aligned}
{}^{t}\vec{V}_1^i &= \frac{\vec{\mathrm{e}}_2 \times {}^{t}\vec{V}_n^i}{\left|\vec{\mathrm{e}}_2 \times {}^{t}\vec{V}_n^i\right|}\\
{}^{t}\vec{V}_2^i &= {}^{t}\vec{V}_n^i \times {}^{t}\vec{V}_1^i
\end{aligned} \tag{8}$$

Substituting Equations (4) and (7) into Equation (3), the incremental displacement vector is obtained. It is worth mentioning that the incremental displacement field can be divided into linear and quadratic parts as follows:

$$\vec{u}(r,s,t) = \overrightarrow{u_l}(r,s,t) + \overrightarrow{u_q}(r,s,t) \tag{9}$$

where

$$\begin{aligned}
\vec{u}_l(r,s,t) &= \sum_{i=1}^{m} h_i(r,s)\overrightarrow{u_i} + \frac{t}{2}\sum_{i=1}^{m} h_i\left({}^0a_i \overset{t\to i}{V_n} i\Delta_a^i - {}^t a_i \overset{t\to i}{V_2} i\alpha_i + {}^t a_i \overset{t\to i}{V_1} i\beta_i\right) \\
&\quad + t^2\sum_{i=1}^{m} h_i(r,s)^0 a_i\left(\overset{t\to i}{V_n} q_n^i - {}^t Q_n^i \overset{t\to i}{V_2}\alpha_i + {}^t Q_n^i \overset{t\to i}{V_1}\beta_i\right) \\
\vec{u}_q(r,s,t) &= \frac{t}{2}\sum_{i=1}^{m} h_i\left[-{}^0a_i \overset{t\to i}{V_2}\Delta_a^i\alpha_i + {}^0a_i \overset{t\to i}{V_1}\Delta_a^i\beta_i - \frac{1}{2}{}^t a_i \overset{t\to i}{V_n}\left(\alpha_i^2+\beta_i^2\right)\right] \\
&\quad + t^2\sum_{i=1}^{m} h_i(r,s)^0 a_i\left[-\overset{t\to i}{V_2} q_n^i\alpha_i + \overset{t\to i}{V_1} q_n^i\beta_i - \frac{1}{2}{}^t Q_n \overset{t\to i}{V_n}\left(\alpha_i^2+\beta_i^2\right)\right]
\end{aligned} \tag{10}$$

3. Strain interpolation

The covariant Green–Lagrange strain tensor is calculated by using the next formula:

$${}^t_0\varepsilon_{ij} = \frac{1}{2}\left({}^t\vec{g}_i\cdot{}^t\vec{g}_j - {}^0\vec{g}_i\cdot{}^0\vec{g}_j\right) \tag{11}$$

Here, the covariant base vector of the element in the convected coordinate system r_i ($r_1 = r,\ r_2 = s,\ r_3 = t$) are as follows:

$$\begin{aligned}
{}^0\vec{g}_i &= \frac{\partial^0\vec{x}}{\partial r_i} \\
{}^t\vec{g}_i &= \frac{\partial^t\vec{x}}{\partial r_i} = \frac{\partial^0\vec{x}}{\partial r_i} + \frac{\partial^t\vec{u}}{\partial r_i} = {}^0\vec{g}_i + {}^t\vec{u}_{,i}
\end{aligned} \tag{12}$$

The incremental covariant strains are obtained as follows:

$$\begin{aligned}
{}_0\varepsilon_{ij} &= {}^{t+\Delta t}_0\varepsilon_{ij} - {}^t_0\varepsilon_{ij} \\
{}_0\varepsilon_{ij} &= \tfrac{1}{2}\left(\vec{u}_{,i}\cdot{}^t\vec{g}_j + {}^t\vec{g}_i\cdot\vec{u}_{,j} + \vec{u}_{,i}\cdot\vec{u}_{,j}\right)
\end{aligned} \tag{13}$$

Equation (13) can be split into linear and nonlinear parts as follows:

$$\begin{aligned}
{}_0e_{ij} &= \tfrac{1}{2}\left(\frac{\partial\vec{u}_l}{\partial r_i}\cdot{}^t\vec{g}_j + {}^t\vec{g}_i\cdot\frac{\partial\vec{u}_l}{\partial r_j}\right) = B_{ij}\vec{U} \\
{}_0\eta_{ij} &= \tfrac{1}{2}\left(\frac{\partial\vec{u}_l}{\partial r_i}\cdot\frac{\partial\vec{u}_l}{\partial r_j}\right) + \tfrac{1}{2}\left(\frac{\partial\vec{u}_q}{\partial r_i}\cdot{}^t\vec{g}_j + {}^t\vec{g}_i\cdot\frac{\partial\vec{u}_q}{\partial r_j}\right) = \tfrac{1}{2}\vec{U}^T N_{ij}\vec{U}
\end{aligned} \tag{14}$$

where B_{ij} and N_{ij} express the linear and nonlinear strain-displacement matrices, respectively. Moreover, $\vec{U}$ is the nodal incremental displacement vector. In order to derive locking free elements, the MITC formulation is

employed. In this scheme, the assumed strains are obtained by interpolating the displacement based strains at tying points as follows (Lee & Bathe, 2004):

$$\hat{\varepsilon}_{ij}(r,s,t) = \sum_{k=1}^{m} h_{ij}^{k}(r,s)\varepsilon_{ij}\Big|_{\left(r_{ij}^{k},s_{ij}^{k},t\right)} \tag{15}$$

For the six-node triangular element, both the in-plane and transverse shear strains are interpolated, while only transverse shear strains' interpolation is required for the three-node element. The functions used for interpolating in-plane strains of the six-node element are defined as follows:

$$\begin{aligned}
\hat{\varepsilon}_{rr} &= \overline{a_1} + \overline{b_1}r + \overline{c_1}s \\
\hat{\varepsilon}_{ss} &= \overline{a_2} + \overline{b_2}r + \overline{c_2}s \\
\hat{\varepsilon}_{qq} &= \overline{a_3} + \overline{b_3}r + \overline{c_3}(1-r-s)
\end{aligned} \tag{16}$$

where

$$\begin{aligned}
&\overline{a_1} = m_{rr}^{(1)} - l_{rr}^{(1)}\,, \quad \overline{b_1} = 2l_{rr}^{(1)}\,, \quad \overline{c_1} = \sqrt{3}\left(\varepsilon_{crr}^{(1)} - \overline{a_1} - \overline{b_1}r_1\right) \\
&\overline{a_2} = m_{ss}^{(2)} - l_{ss}^{(2)}\,, \quad \overline{b_2} = \sqrt{3}\left(\varepsilon_{css}^{(2)} - \overline{a_2} - \overline{c_2}s_1\right)\,, \quad \overline{c_2} = 2l_{ss}^{(2)} \\
&\overline{a_3} = m_{qq}^{(3)} - l_{qq}^{(3)}\,, \quad \overline{b_3} = -2l_{qq}^{(3)}\,, \quad \overline{c_3} = \sqrt{3}\left(\varepsilon_{cqq}^{(3)} - \overline{a_3} - \overline{b_3}r_1\right) \\
&m_{jj}^{(i)} = \frac{1}{2}\left(\varepsilon_{1jj}^{(i)} + \varepsilon_{2jj}^{(i)}\right)\,, \quad l_{jj}^{(i)} = \frac{\sqrt{3}}{2}\left(\varepsilon_{2jj}^{(i)} - \varepsilon_{1jj}^{(i)}\right) : \; j = r,s,q \qquad i = 1,2,3
\end{aligned} \tag{17}$$

On the other hand, the interpolation functions of the transverse shear strains have the following form:

$$\begin{aligned}
\hat{\varepsilon}_{rt} &= \overline{\overline{a_1}} + \overline{\overline{b_1}}r + \overline{\overline{c_1}}s + \overline{\overline{d_1}}rs + \overline{\overline{f_1}}s^2 \\
\hat{\varepsilon}_{st} &= \overline{\overline{a_2}} + \overline{\overline{b_2}}r + \overline{\overline{c_2}}s + \overline{\overline{d_2}}rs + \overline{\overline{f_2}}r^2
\end{aligned} \tag{18}$$

The required coefficients are defined as follows:

$$\begin{aligned}
&\overline{\overline{a_1}} = m_{rt}^{(1)} - l_{rt}^{(1)}, \;\; \overline{\overline{b_1}} = 2l_{rt}^{(1)} \;\;, \;\; \overline{\overline{c_1}} = 6\varepsilon_{crt} - 3\varepsilon_{cst} + 2m_{st}^{(3)} - 2m_{rt}^{(3)} - 4\overline{\overline{a_1}} - \overline{\overline{b_1}} + \overline{\overline{a_2}} \\
&\overline{\overline{a_2}} = m_{st}^{(2)} - l_{st}^{(2)}, \;\; \overline{\overline{b_2}} = -3\varepsilon_{crt} + 6\varepsilon_{cst} - 2m_{st}^{(3)} + 2m_{rt}^{(3)} + \overline{\overline{a_1}} - 4\overline{\overline{a_2}} - \overline{\overline{c_2}}, \quad \overline{\overline{c_2}} = 2l_{st}^{(2)} \\
&\overline{\overline{f}}_1 = -6\varepsilon_{crt} + 3\varepsilon_{cst} - 3m_{st}^{(3)} - l_{st}^{(3)} + 3m_{rt}^{(3)} + l_{rt}^{(3)} + 3\overline{\overline{a_1}} + \overline{\overline{b_1}} + \overline{\overline{c_2}} \\
&\overline{\overline{f}}_2 = 3\varepsilon_{crt} - 6\varepsilon_{cst} + 3m_{st}^{(3)} - l_{st}^{(3)} - 3m_{rt}^{(3)} + l_{rt}^{(3)} + \overline{\overline{b_1}} + 3\overline{\overline{a_2}} + \overline{\overline{c_2}} \\
&\overline{\overline{d_1}} = -\overline{\overline{f_2}} \quad , \quad \overline{\overline{d_2}} = -\overline{\overline{f_1}} \\
&m_{jt}^{(i)} = \frac{1}{2}\left(\varepsilon_{1jt}^{(i)} + \varepsilon_{2jt}^{(i)}\right)\,, \quad l_{jt}^{(i)} = \frac{\sqrt{3}}{2}\left(\varepsilon_{2jt}^{(i)} - \varepsilon_{1jt}^{(i)}\right) : \qquad j = r,s \qquad i = 1,2,3
\end{aligned} \tag{19}$$

For three-node element, the following relations are held:

$$\begin{aligned}\hat{\varepsilon}_{rt} &= \varepsilon_{rt}^{(1)} + cs\,,\ \hat{\varepsilon}_{st} = \varepsilon_{st}^{(2)} - cr \\ c &= \varepsilon_{st}^{(2)} - \varepsilon_{rt}^{(1)} - \varepsilon_{st}^{(3)} + \varepsilon_{rt}^{(3)}\end{aligned} \tag{20}$$

Based on Equation (16), the interpolation function of the in-plane shear strain is obtained as follows:

$$\hat{\varepsilon}_{rs} = \frac{1}{2}(\hat{\varepsilon}_{rr} + \hat{\varepsilon}_{ss}) - \hat{\varepsilon}_{qq} \tag{21}$$

The tying point positions of three- and six-node elements are defined in Figure 2 and Table 1.

In order to alleviate the thickness locking phenomena, the following interpolation is used for transverse normal strain (Kim & Bathe, 2008).

$$\hat{\varepsilon}_{33}(r,s,t) = \sum_{k=1}^{m} h_k(r_k,s_k)\varepsilon_{33}|_{(r_k,s_k,t=0)} + \left(\varepsilon_{33}|_{(r,s,t)} - \varepsilon_{33}|_{(r,s,t=0)}\right) \tag{22}$$

4. Linearised governing equation

In conjunction with Total Lagrangian formulation, the principle of virtual work is utilised to obtain the variational governing equation. After linearisation, the following incremental equation is available:

$$\int_{{}_0V} {}_0\tilde{C}^{ijkl}\,{}_0\tilde{e}_{kl}\,\delta_0\,\tilde{e}_{ij}\,{}^0dV + \int_{{}_0V} {}^t_0\tilde{S}^{ij}\delta_0\,\tilde{\eta}_{ij}\,{}^0dV = {}^{t+\Delta t}\Re - \int_{{}_0V} {}^t_0\tilde{S}^{ij}\,\delta_0\,\tilde{e}_{ij}\,{}^0dV \tag{23}$$

where ${}^t_0\tilde{S}^{ij}$ is the second Piola–Kirchhoff stress tensor. Moreover, ${}_0\tilde{e}_{ij}$ and ${}_0\tilde{\eta}_{ij}$ are the linear and nonlinear terms of Green–Lagrange strain tensor, respectively. The fully 3D stress–strain relation is depicted by ${}_0\tilde{C}^{ijkl}$ in

Table 1. The tying points positions.

Element	ε	r	s
Three-node	$\varepsilon_{rt}^{(1)}$	$1/2$	0
	$\varepsilon_{st}^{(2)}$	0	$1/2$
	$\varepsilon_{rt}^{(1)}$, $\varepsilon_{st}^{(2)}$	$1/2$	$1/2$
Six-node	ε_{crt}, ε_{cst}	$1/3$	$1/3$
	$\varepsilon_{1rr}^{(1)}$, $\varepsilon_{1rt}^{(1)}$	$1/2 - 1/2\sqrt{3}$	0
	$\varepsilon_{1ss}^{(2)}$, $\varepsilon_{1st}^{(2)}$	0	$1/2 - 1/2\sqrt{3}$
	$\varepsilon_{cqq}^{(3)}$	$1/2 - 1/2\sqrt{3}$	$1/2 - 1/2\sqrt{3}$
	$\varepsilon_{2rr}^{(1)}$, $\varepsilon_{2rt}^{(1)}$	$1/2 + 1/2\sqrt{3}$	0
	$\varepsilon_{2ss}^{(2)}$, $\varepsilon_{2st}^{(2)}$	0	$1/2 + 1/2\sqrt{3}$
	$\varepsilon_{2qq}^{(3)}$, $\varepsilon_{2qt}^{(3)}$	$1/2 - 1/2\sqrt{3}$	$1/2 + 1/2\sqrt{3}$
	$\varepsilon_{1qq}^{(3)}$, $\varepsilon_{1qt}^{(3)}$	$1/2 + 1/2\sqrt{3}$	$1/2 - 1/2\sqrt{3}$
	$\varepsilon_{crr}^{(1)}$	$1/2 - 1/2\sqrt{3}$	$1/\sqrt{3}$
	$\varepsilon_{css}^{(2)}$	$1/\sqrt{3}$	$1/2 - 1/2\sqrt{3}$

global Cartesian coordinates. The components of the constitutive matrix in the local curvilinear system are defined and transformed as follows:

$$\widehat{C}^{mnop} = \frac{E}{\Delta}\begin{bmatrix} 1-\nu & \nu & \nu & 0 & 0 & 0 \\ & 1-\nu & \nu & 0 & 0 & 0 \\ & & 1-\nu & 0 & 0 & 0 \\ & & & \frac{1}{2}-\nu & 0 & 0 \\ & sym & & & \frac{1}{2}-\nu & 0 \\ & & & & & \frac{1}{2}-\nu \end{bmatrix} \quad \Delta = (1-2\nu)(1+\nu)$$

$$\tilde{C}^{ijkl} = \left(\vec{g}^{\,i}.\vec{e}_m\right)\left(\vec{g}^{\,j}.\vec{e}_n\right)\left(\vec{g}^{\,k}.\vec{e}_o\right)\left(\vec{g}^{\,l}.\vec{e}_p\right)\widehat{C}^{mnop} \tag{24}$$

Substituting the incremental relations in terms of degrees of freedom into Equation (23), the finite-element form of the governing equation can be obtained as follows:

$$\left({}^{t}_{0}K_L + {}^{t}_{0}K_{NL}\right)\vec{q} = {}^{t+\Delta t}\Re - {}^{t}_{0}F \tag{25}$$

where $\vec{q}$ is the vector of nodal displacement. ${}^{t}_{0}F$and ${}^{t+\Delta t}\Re$ are the internal and external forces, respectively.

5. Numerical study

To show the capability of the proposed elements, four problems are studied and the results are compared with those available in the literatures. It should be mentioned that 7 Gauss points have been employed for the in-plane direction, and the number of Gauss's points used across the thickness direction was equal to 4. The nonlinear solution method, which is employed in this study, is Generalised Displacement Control Method (GDCM). The convergence is assumed to be reached whenever the ratio of the residual force norm to the external force norm is less than the tolerance criteria. Note that all units used for force and lengths are reported in *N* and *mm*, respectively.

5.1. *A cantilever plate*

As a first example, a convergence study is considered for a cantilever plate, which is depicted in Figure 3. Solving this problem shows the high performance and accuracy of the proposed elements. It is aimed to illustrate the capability of the authors' scheme in the linear analysis of thin and thick plate structures, as well. In addition, the effects of considering thickness-stretching as a degree of freedom are investigated, separately. First, convergence study is implemented to reach the optimum number of triangular shell elements. Then, the structure is solved for different thickness values to investigate the effect of thickness on the deflection responses.

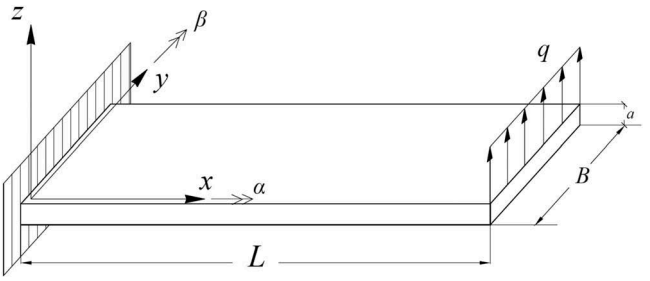

Figure 3. A cantilever plate under the end distributed shear force.

The beam length is equal to 10. The mechanical and geometrical properties of plate are as follows:$E = 1.2 \times 10^6\,\text{MPa}$, $v = 0.0$ *and* $B = 1.0\,mm$. As it is shown in Figure 3, the maximum distributed load, which is applied at the free end of plate is assumed to be equal to 4. Based on the Timoshenko beam theory, the exact solution of tip displacement for a plate is available as follows:

$$\begin{aligned} G &= \frac{E}{2} = 6 \times 10^5 \text{MPa} \\ w &= \frac{PL^3}{3EI} + \frac{PL}{\kappa AG} = \frac{4 \times 10^3}{3 \times 1.2 \times 10^6 \times \frac{1 \times 0.1^3}{12}} + \frac{4 \times 10}{\frac{5}{6} \times 0.1 \times 1 \times 6 \times 10^5} \\ &= 13.33413mm \end{aligned} \tag{26}$$

Since this theory satisfies the first-order of shear deformation, the responses of five-parameter shell element, which was formulated in Rezaiee-Pajand et al. (2018), are accurate while the proposed the seven-parameter shell element obtains the results with a little difference. It should be noted that 3D stress–strain matrix is employed for deriving the stiffness matrix of seven-parameter while a reduced plane stress constitutive matrix is utilised for stiffness matrix of five-parameter element. This fact is due to consider thickness-stretching effects on the formulation of element. It is observed that by increasing the thickness of plate, the effect of thickness-stretching and the differences of results are more considerable.

Two cases are considered. First, five-parameter element with no thickness-stretching effect is employed for mesh discretisation. Second, seven-parameter shell element, proposed in this paper, is used for modelling. The percentage of differences between two cases is compared with each other in Figure 4 for the various thicknesses. Figure 5 illustrates the convergence curve. This study is performed for three-node triangular shell element. The obtained results show that using 32 triangular shell elements is adequate for finding the near exact solution with

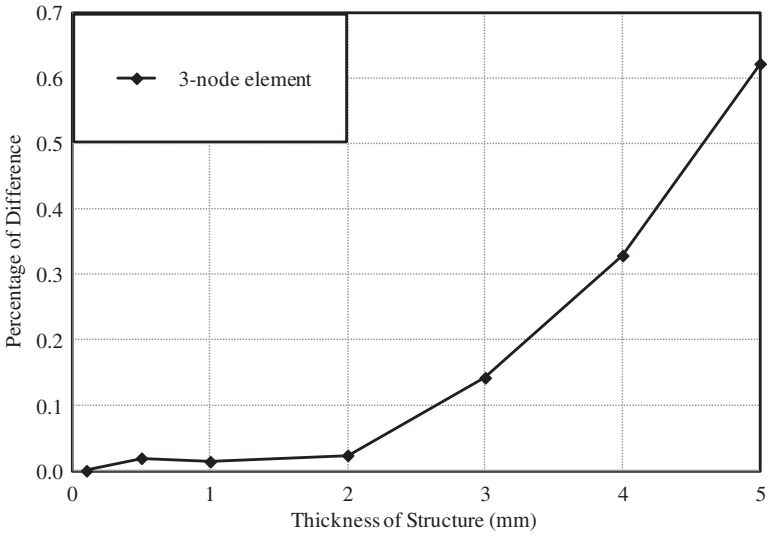

Figure 4. The percentage of differences between five- and seven-parameter shell element versus thickness variation.

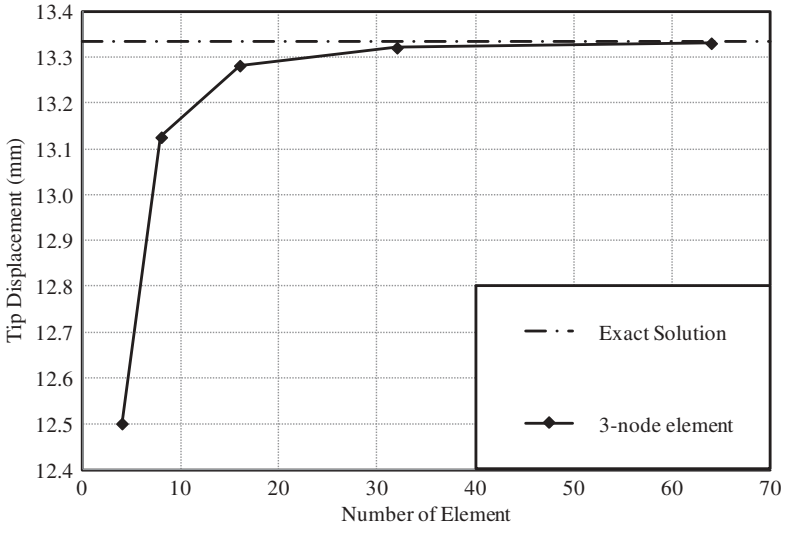

Figure 5. The convergence curve provided for a cantilever plate under the end distributed shear force.

the error of less than 0.1%. This study is performed for a thin shell in which the thickness is equal to 0.1.

5.2. *Slit annular plate*

In this example, a slit annular plate depicted in Figure 6 is analysed. This problem is solved to present that the proposed element is free of locking in

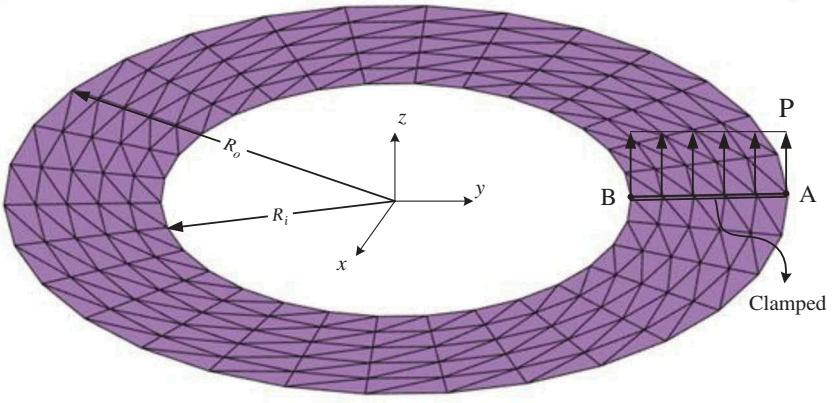

Figure 6. The geometry of slit annular plate.

thin shell structures. In addition, large rotation can be predicted accurately based on the proposed formulation. The inner and outer radius of the plate is equal to 6.0 *mm* and 10.0 mm, respectively. Moreover, one end of the structure is clamped and the other one is free. In addition, a uniform distributed load P, which is equal to 3.2 N, is applied at the free end of the plate. The module of elasticity is equal to $E = 21 \times 10^6$ MPa. The thickness of plate is 0.03 mm. This structure undergoes large displacements and large rotations. To model this plate, a 5×60 and 6×120 mesh discretisation, including 300 and 720 elements, are employed for six-node and three-node element, respectively. These are shown in Figure 6.

The obtained equilibrium path is compared with research's results of Sze, Liu, and Lo (2004). Figure 7 shows the deformed shape of the plate at the final step of loading.

The vertical displacements (W) of the points A and B are depicted in Figure 8. It should be added that the results are obtained for both proposed seven-parameter elements. Due to low thickness of the slit annular plate, the thickness-stretching should not be effective on the responses. This fact is also concluded from the obtained results. Furthermore, the difference between reference solution and results of three-node element is due to the lower capability of the three-node shell element in large rotation analysis. It should be emphasised that this deficiency will be made up by increasing the number of element.

5.3. *Pull-out cylindrical shell*

In this part, the nonlinear behaviour of cylindrical shell under two opposite point loads is investigated. The boundary conditions at the two ends of the structure are assumed to be free. The material and geometrical characteristics employed in this example are as follows:

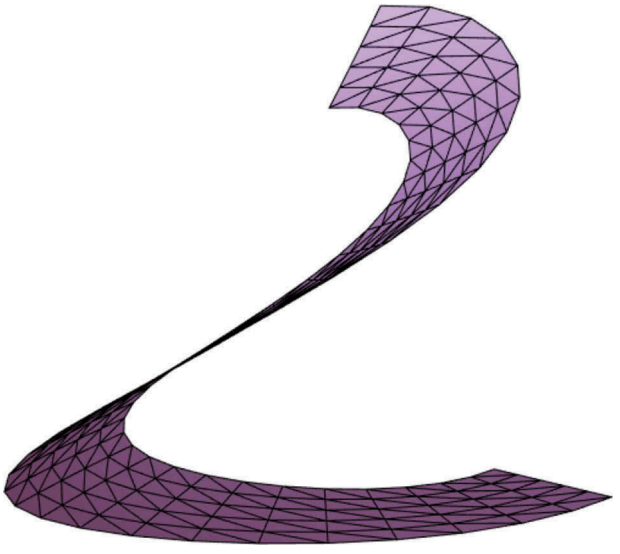

Figure 7. The deformed shape of slit annular plate at the last step of analysis.

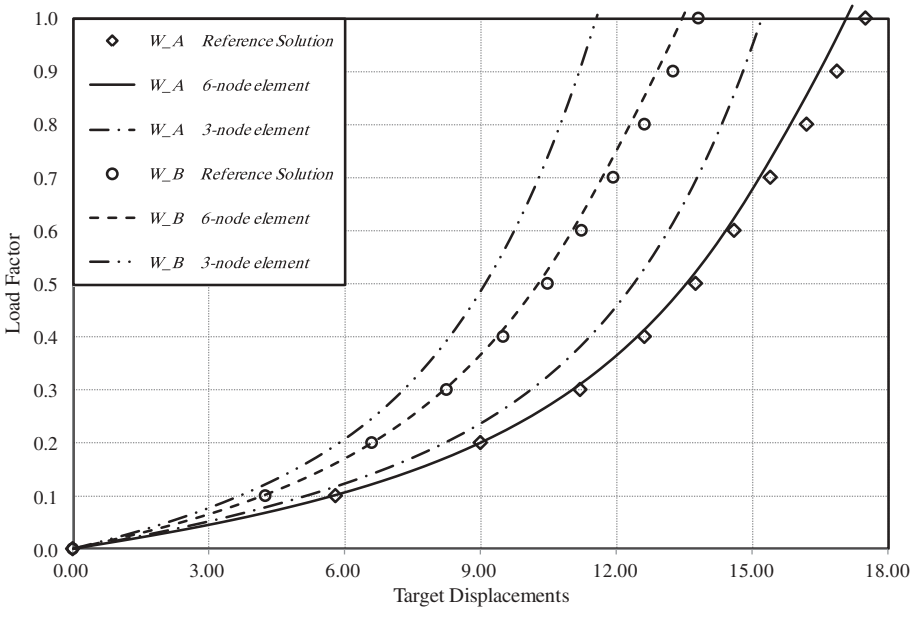

Figure 8. The vertical displacement (mm) of slit annular plate at the points A and B.

$$E = 10.5 \times 10^6 \text{ MPa}, \quad \nu = 0.3125$$
$$L = 10.35\,mm, R = 4.953\,mm, \quad a = 0.094\,mm \tag{27}$$

Taking advantage of the structure symmetry, only an octant of cylindrical shell is considered by utilising 10 × 10 × 2 mesh discretisation for both proposed elements. As it is shown in Figure 9, the displacements are

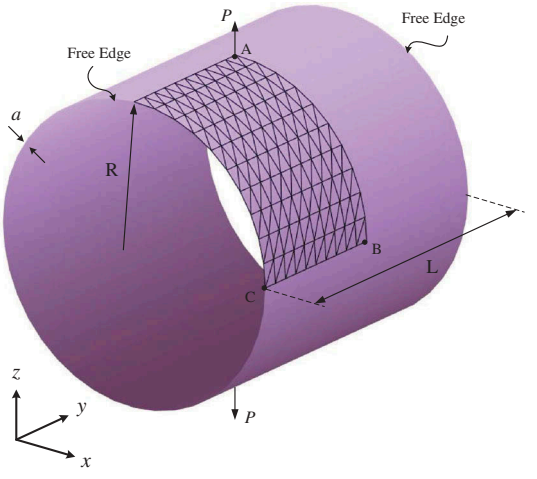

Figure 9. The geometry and mesh description of cylindrical shell.

obtained for three points, including w_A, u_B and u_C. It is obvious that w and u are the displacements along z- and x-directions, respectively.

The results of both three- and six-node elements and those reported in Arciniega & Reddy (2007; Sze et al., 2004) and are demonstrated in Figure 10.

The comparison of obtained results with the reference solutions shows good agreement. However, there are some differences between the responses of three-node element discretisation and the reference solution, in particular, when the load factor is >0.5. This is because the lower-order polynomial has been employed in the formulation of the three-node

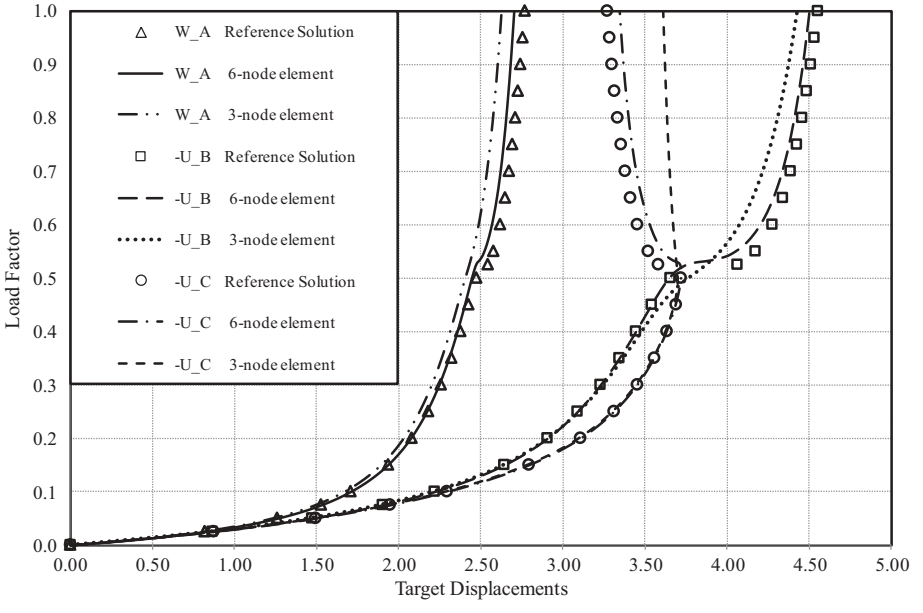

Figure 10. Displacement responses (mm) of cylindrical shell at points of A, B, and C.

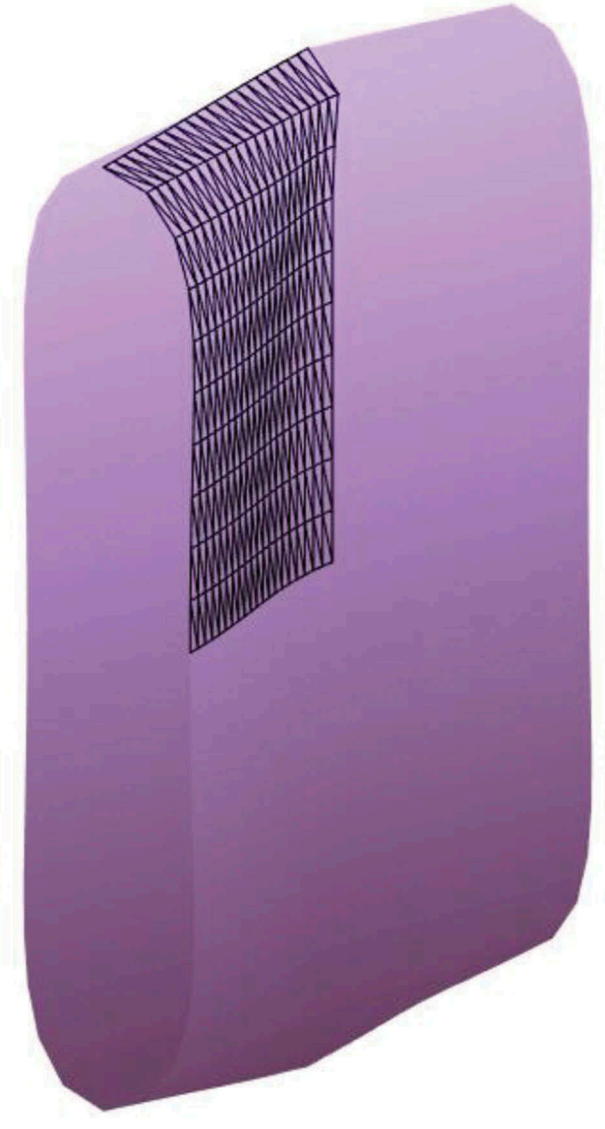

Figure 11. Deformed shape of pull-out cylindrical shell at the end of loading.

element. Figure 11 demonstrates the deformed shape of cylindrical shell at the end of loading.

5.4. *Shallow panel under point load*

A shallow panel is analysed here by considering the thickness-stretching effects. Figure 12 shows the mesh pattern and geometry of the structure under a concentrated load at the centre of the shell. The number of three- and six-node shell elements that are used for this modelling is equal to 200

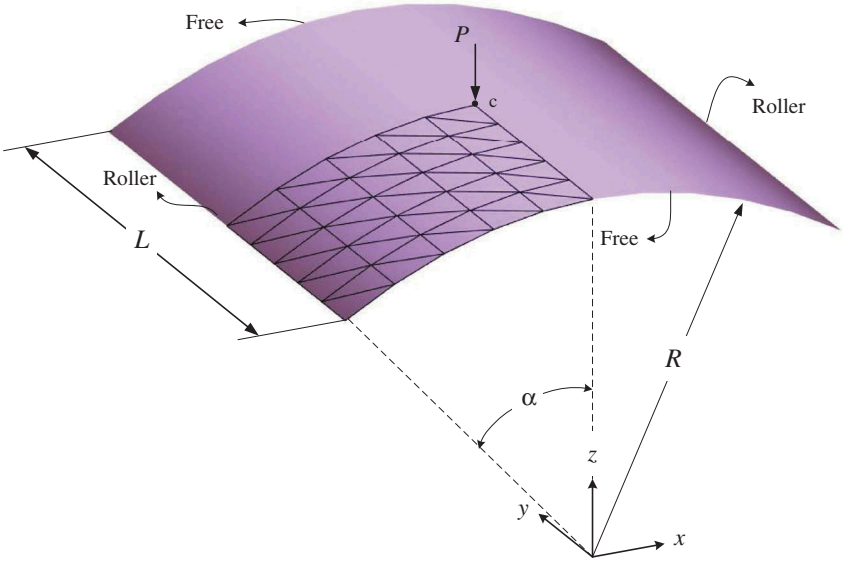

Figure 12. The geometry of shallow panel under the central concentrated load.

and 50, respectively. It should be added that the numbers of total degrees of freedom are the same. The geometry and Mechanical properties of the shallow shell are as follows:

$$\begin{aligned} &a = 12.7\,mm \quad R = 2540\,mm \quad L = 508\,mm \quad \alpha = 0.1\text{rad} \\ &v = 0.3 \quad E = 3102.75\,\text{MPa} \end{aligned} \tag{28}$$

Due to the structural symmetry, a quarter of the shallow shell is considered for analysis. It should be noted that various thicknesses including 6.35 mm, 12.7 mm, and 25.4 mm are employed for modelling this shallow structure. The effects of these thicknesses, along the equilibrium path of the vertical displacement, and thickness variation, are studied. It is expected that the variation of vertical displacement for the lower thickness shell is the same as the reference solution (Arciniega & Reddy, 2007), because the effects of thickness-stretching on the deflection of the thin shell can be ignored. This fact is completely proven in this example. Moreover, the results of vertical displacement versus load factor are obtained in Figures 13–15. It should be added that the responses are provided for both proposed three- and six-node elements. In Figures 13 and 14, authors' responses are compared with the reference solution for the thicknesses of 6.35 *mm* and 12.7 *mm* (Arciniega & Reddy, 2007).

Figure 16 shows the rate of thickness variation versus load factors for various thicknesses of the shell. To verify the solution, two mesh patterns, including 50 and 200, for the six-node shell element are employed for the case of 25.4-mm thickness. It is observed that the responses do not change

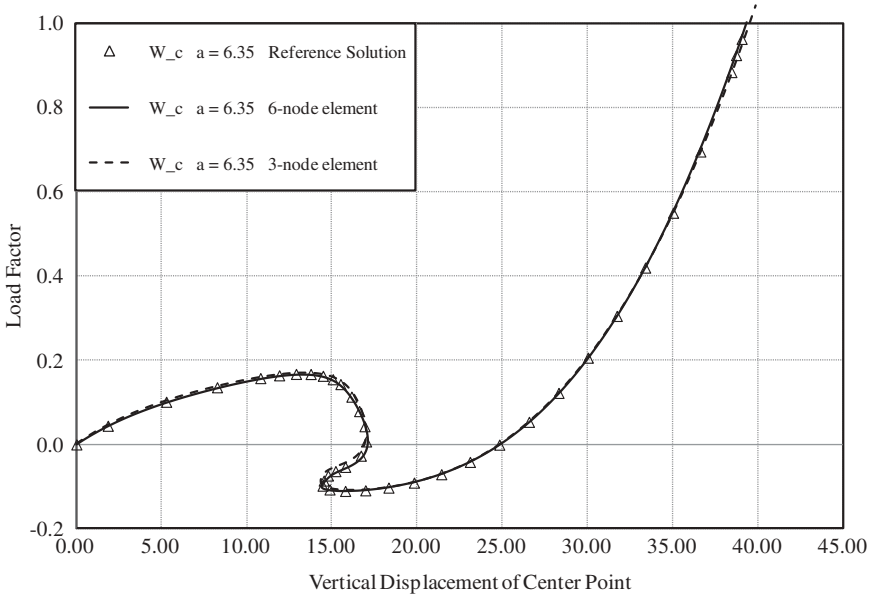

Figure 13. The equilibrium path of shallow panel with the thickness of 6.35 mm.

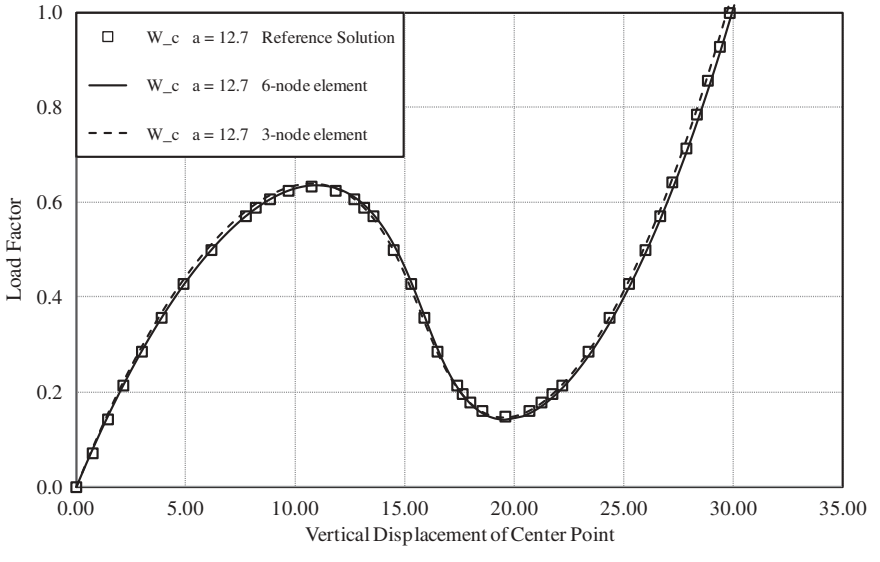

Figure 14. The equilibrium path of shallow panel with the thickness of 12.7 mm.

by refining the mesh discretisation. Therefore, it can be concluded that the obtained results are reliable.

According to Figure 16, it can be concluded that the rate of thickness variation for the thicker shell is more considerable than that of the thin one. It is obvious that the effect of ε_{zz} can be negligible for the thin

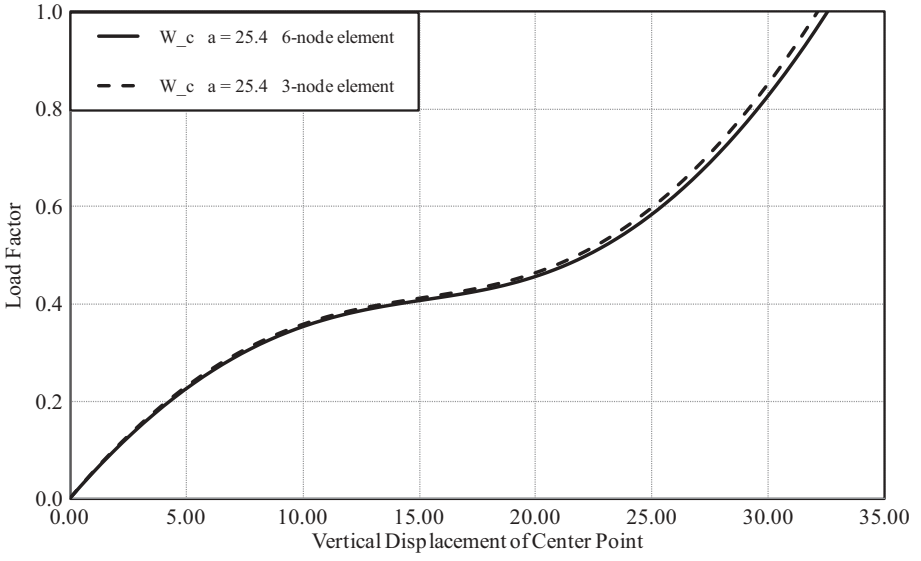

Figure 15. The equilibrium path of shallow panel with the thickness of 25.4 mm.

shells. The deformed shape of shallow shells at the last step of loading is illustrated in Figure 17.

5.5. *Clamped plate under central uniform distributed load*

The objective of this example is to analyse a clamped plate. The two ends of plate are considered to be fixed. The boundary conditions and geometry of structure are shown in Figure 18. The plate undergoes a uniform distributed load (q) with the value of 64,000 N/mm, which is applied per unit of undeformed surface of plate. Due to considering the thickness effects on the results, three different thicknesses, including 0.3 mm, 0.625 mm, and 1.2 mm, are employed here. The geometry and mechanical properties are as follows:

$$\begin{aligned} &L = 12.0\,mm \quad B = 1.0\,mm \quad a = 0.3\,mm, 0.625\,mm \quad \text{and } 1.20\,mm \\ &v = 0.3 \qquad E = 10^7\,\text{MPa} \end{aligned} \tag{29}$$

The number of three- and six-node shell elements that are used for discretisation is equal to 32. Figure 19 illustrates the structural equilibrium path of the central deflection for different thicknesses. The results are provided for both proposed elements.

It can be observed that there is a good agreement between the results obtained by two elements. Figure 20 reports the rate of thickness variation versus load factors. It is noticeable that this parameter is increased in the thicker plates. As it is demonstrated, the deformed shape of plate at the last step of load is shown in Figure 21.

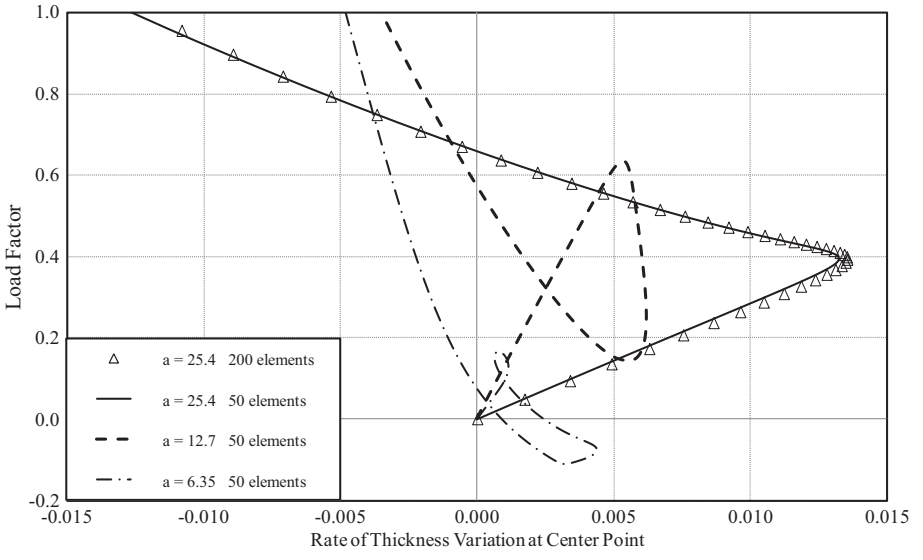

Figure 16. The rate of thickness variation versus load factors for shallow panel.

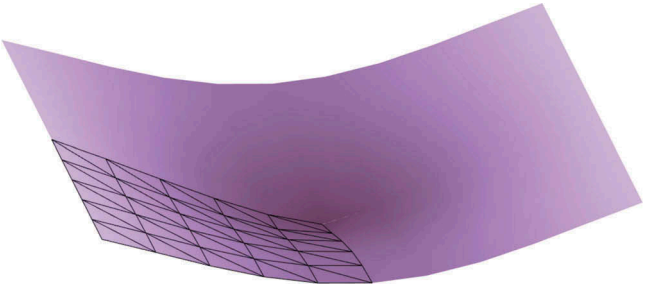

Figure 17. Deformed shape of shallow panel at the end of loading.

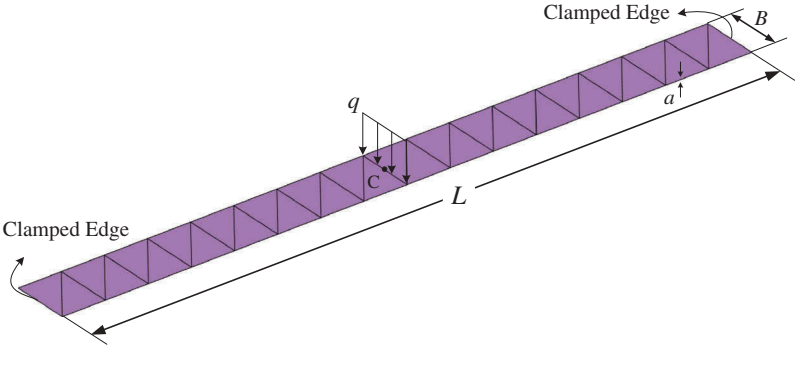

Figure 18. The geometry and mesh discretisation of clamped plate under central uniform load.

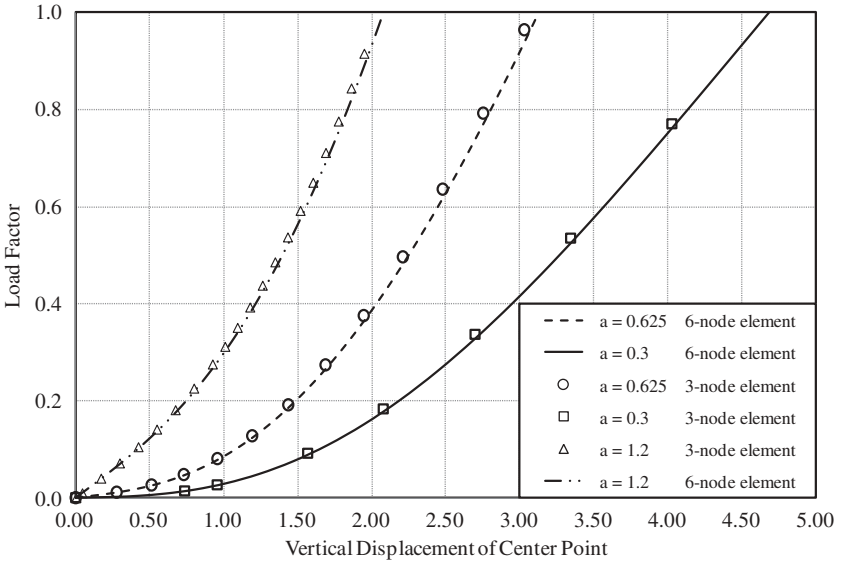

Figure 19. The equilibrium path of clamped plate under central concentrated load at point C.

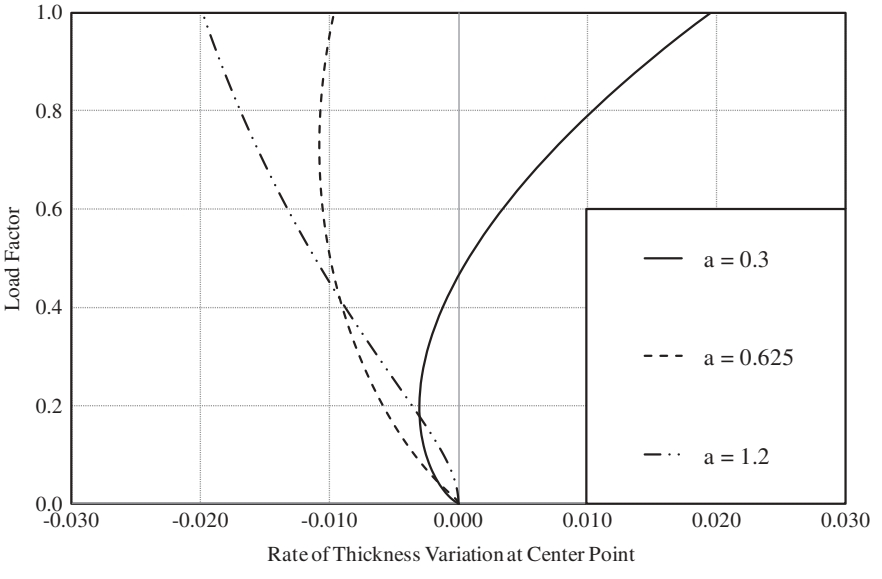

Figure 20. The rate of thickness vibration versus load factors for clamped plate under a central point load.

6. Conclusions

The main objective of this research was proposing two seven-parameter triangular shell elements for the geometrically nonlinear analysis of the thin and thick shell structures. Two shell elements, with three and six nodes were formulated. In order to model the thickness variation, two

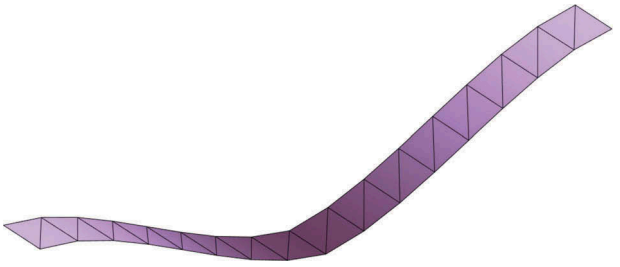

Figure 21. Deformed shape of clamped plate under the central distributed load at the end of loading.

additional degrees of freedom were used at each node. It is worth mentioning, the fully 3D constitutive relation was utilised in authors' formulation. To resolve numerical problems, such as, membrane, shear and thickness locking, the MITC method was applied in this study. Based on the obtained results, it can be concluded that the effects of the thickness-stretching are more considerable as the thickness of the shell increases. The validity and accuracy of proposed elements were determined by comparing the results with the findings of the other researchers.

Disclosure statement

No potential conflict of interest was reported by the authors.

References

Ahmad, S., Irons, B., & Zienkiewicz, O. C. (1970). Analysis of thick and thin shell structures by curved finite elements. *International Journal for Numerical Methods in Engineering*, *2*(3), 419–451.

Arciniega, R. A., & Reddy, J. N. (2007). Tensor-based finite element formulation for geometrically nonlinear analysis of shell structures. *Computer Methods in Applied Mechanics and Engineering*, *196*, 1048–1073.

Bathe, K. J. (1982). *Finite element procedures in engineering analysis*. Engiewood Cliffs, NJ: Prentice-Hall.

Boutagouga, D., Gouasmia, A., & Djeghaba, K. (2010). Geometrically nonlinear analysis of thin shell by a quadrilateral finite element with in-plane rotational degrees of freedom. *European Journal of Computational Mechanics*, *19*(8), 707–724.

Bucalem, M. L., & Bathe, K. J. (1993). Higher-order MITC general shell element. *International Journal for Numerical Methods in Engineering*, *36*, 3729–3754.

Buchter, N., Ramm, E., & Roehl, D. (1994). Three-dimensional extension of nonlinear shell formulation based on the enhanced assumed strain concept. *International Journal for Numerical Methods in Engineering*, *37*, 2551–2568.

Chapelle, D., & Bathe, K. J. (2011). *The finite element analysis of shells – fundamentals*. New York, NY: Springer.

Coda, H. B., & Paccola, R. R. (2007). An alternative positional FEM formulation for geometrically non-linear analysis of shells: Curved triangular isoparametric elements. *Computational Mechanics*, *40*, 185–200.

Crisfield, M. (1986). *Finite elements on solution procedures for structural analysis, (I) linear analysis*. Swansea: Pineridge Press.

Dung, N. T., & Wells, G. N. (2008). Geometrically nonlinear formulation for thin shells without rotation degrees of freedom. *Computer Methods in Applied Mechanics and Engineering*, *197*, 2778–2788.

Dvorkin, E. N. (1995). Nonlinear analysis of shells using the MITC formulation. *Archives of Computational Methods in Engineering*, *2*(2), 1–50.

Dvorkin, E. N., & Bathe, K. J. (1984). A continuum mechanics based four-node shell node shell element for general nonlinear analysis. *Engineering Computations*, *1*(1), 77–88.

El-Abbasi, N., & Meguid, S. A. (2000). A new shell element accounting for through-thickness deformation. *Computer Methods in Applied Mechanics and Engineering*, *189*, 841–862.

Jeon, H.-M., Lee, Y., Lee, P.-S., & Bathe, K.-J. (2015). The MITC3+ shell element in geometric nonlinear analysis. *Computers & Structures*, *146*, 91–104.

Jung, W.-Y., & Han, S.-C. (2015). A refined element-based Lagrangian shell element for geometrically nonlinear analysis of shell structures. *Advances in Mechanical Engineering*, *7*(4), 1–19.

Kim, D.-N., & Bathe, K.-J. (2008). A 4-node 3D-shell element to model shell surface tractions and incompressible behavior. *Computers and Structures*, *86*, 2027–2041.

Kordkheili, S. A. H., Naghdabadi, R., & Jabbarzadeh, M. (2008). A geometrically nonlinear finite element formulation for shells using a particular linearization method. *Finite Elements in Analysis and Design*, *44*(3), 123–130.

Lee, P. S., & Bathe, K. J. (2004). Development of MITC isotropic triangular shell finite elements. *Computers and Structures*, *82*, 945–962.

Lee, Y., Lee, P.-S., & Bathe, K.-J. (2014). The MITC3+ shell element and its performance. *Computers & Structures*, *138*, 12–23.

Li, Z., & Vu-Quoc, L. (2007). An efficient co-rotational formulation for curved triangular shell element. *International Journal for Numerical Methods in Engineering*, *72*, 1029–1062.

Liu, W. K., Law, E. S., Lam, D., & Belytschko, T. (1986). Resultant-stress degenerated-shell element. *Computer Methods in Applied Mechanics and Engineering*, *55*(3), 259–300.

Masoodi, A. R., & Arabi, E. (2018). Geometrically nonlinear thermomechanical analysis of shell-like structures. *Journal of Thermal Stresses*, *41*(1), 37–53.

Nguyen-Van, H., Nguyen-Hoai, N., Chau-Dinh, T., & Tran-Cong, T. (2015). Large deflection analysis of plates and cylindrical shells by an efficient four-node flat element with mesh distortions. *Acta Mechanica*, *226*(8), 2693–2713.

Pimenta, P. M., Campello, E. M. B., & Wriggers, P. (2004). A fully nonlinear multi-parameter shell model with thickness variation and a triangular shell finite element. *Computational Mechanics*, *34*, 181–193.

Rezaiee-Pajand, M., Arabi, E., & Masoodi, A. R. (2018). A triangular shell element for geometrically nonlinear analysis. *Acta Mechanica*, *229*(1), 323–342.

Surana, K. S. (1982). Geometrically nonlinear formualtion for the three dimensional solid-shell transition finite element. *Comouters and Structures*, *15*(5), 549–566.

Sze, K. Y., Liu, X. H., & Lo, S. H. (2004). Popular benchmark problems for geometric nonlinear analysis of shells. *Finite Elements in Analysis and Design*, *40*, 1551–1569.